Magnetic Resonance in Medicine 41:1199–1205 (1999)

High Spatial Resolution EPI Using an Odd Number of Interleaves

Michael H. Buonocore* and David C. Zhu

Ghost artifacts in echoplanar imaging (EPI) arise from phase errors caused by differences in eddy currents and gradient ramping during left-to-right traversal of k_x (forward echo) versus right-to-left traversal of k_x (reverse echo). Reference scans do not always reduce the artifact and may make image quality worse. To eliminate the need for reference scans, a ghost artifact reduction technique based on image phase correction was developed, in which phase errors are directly estimated from images reconstructed separately using only the forward or only the reverse echos. In practice, this technique is applicable only to single-shot EPI that produces only one ghost (shifted ½ the field of view from the parent image), because the technique requires that the ghosts do not completely overlap the parent image. For higher spatial resolution, typically an even number of separate k-space traversals (interleaves) are combined to produce one large data set. In this paper, we show that data obtained from an even number of interleaves cannot be combined to produce only one ghost, and image phase correction cannot be applied. We then show that data obtained from an odd number of interleaves can be combined to produce only one ghost, and image phase correction can be applied to reduce ghost intensity significantly. This "odd-number interleaf EPI" provides spatial and temporal resolution tradeoffs that are complementary to, or can replace, those of even-number interleaf EPI. Odd-number interleaf EPI may be particularly useful for MR systems in which reference scans have been unreliable. Magn Reson Med 41:1199–1205, 1999. © **1999 Wiley-Liss, Inc.**

Key words: magnetic resonance imaging; interleaved echo planar imaging; ghost artifact suppression; image phase correction

To increase spatial resolution in echoplanar imaging (EPI), two or more separate k-space traversals (interleaves) can be used to acquire different sets of k-space lines that are combined to produce one large data set. Typically, this "interleaved EPI" uses an even number of interleaves (1–4). Interleaved EPI is particularly sensitive to the generation of ghost artifacts, which arise from the differences in eddy currents and gradient ramping that occur during left-to-right traversal of k_x (forward echo, denoted *l*) versus right-to-left traversal of k_x (reverse echo, denoted *r*). These forward and reverse echos cause different phase errors that result, upon two-dimensional (2D) Fourier transformation, in ghost artifacts in the phase encode (k_y) direction. These ghosts can often be reduced using phase error information obtained from non-k_y encoded reference scans (5–11).

Previously, one of the authors published a ghost artifact reduction technique (12) based on extracting the spatially dependent phase errors directly from images reconstructed separately using only the forward or only the reverse echos. This technique was developed only for single-shot EPI, in which forward and reverse echos are alternated in k-space, and Fourier reconstruction produces a single ghost artifact shifted by ½ the field of view (FOV) from the location of the "parent" image. The technique requires, for each location in the frequency encode direction, at least one pixel within the parent image that the ghost artifact does not overlap. The technique could not be applied to even-number interleaf EPI that have been presented in the literature, because the multiple ghost artifacts produced in these scans entirely overlapped the parent image. With h interleaves, ghost and parent images were separated by only $\pm 1/2h$ the FOV.

This paper introduces and illustrates the advantages of using an *odd* number of interleaves. The fundamental criteria for the interleaved EPI sequence design was to achieve a k-space trajectory that mimics the following features of a single-shot EPI method that are critical to producing images without ghost artifacts: 1) smooth T2* decay of the signal as a function of k_y; and 2) phase errors due to forward and reverse echos arranged in an alternating *l-r-l-r-l-r-l-r-etc.* pattern as a function of k_y. Reduction of ghost artifacts from T_2^* decay has been previously addressed in the literature (2). In single-shot EPI, the decay is smooth as a function of k_y and causes only a local blurring of the image. In interleaved EPI, the decay can significantly affect image quality if the combined data set is strongly modulated as a function of k_y. Strong modulation is avoided by temporally delaying each interleaf in accordance with its starting k_y, such that the combined data set acquires a smooth T_2^* decay in the k_y direction. As we will show, the need to assemble a *l-r-l-r-l-r-l-r-etc.* alternation of phase errors in the interleaved EPI data set leads naturally to the use of an odd-number of interleaves. An odd number is necessary to generate a single ghost that is well separated from the parent image and to utilize image phase correction.

THEORY

Let N equal the number of raw data points in the k_x and k_y directions and in the final image. Define $g_{lr}(n)$ according to the direction of the nth k-space line,

$$g_{lr}(n) = \begin{cases} 1 & \text{if } n\text{th line acquired from left to right (forward echo)} \\ -1 & \text{if } n\text{th line acquired from right to left (reverse echo)} \end{cases} \quad [1]$$

and define $\theta(x, y)$ as the phase errors at each echo center (with forward and reverse echos differing in the sign of θ),

Department of Radiology, UC Davis Medical Center, Sacramento, California.

Presented in part at the 6th Annual Meeting of the International Society of Magnetic Resonance in Medicine, April 17–25, 1998, Sydney, Australia.

*Correspondence to: Michael H. Buonocore, Dept. of Radiology, TICON-II, 2nd floor, UC Davis Medical Center, Sacramento, CA 95817.

Received 18 May 1998; revised 21 December 1998; accepted 19 January 1999.

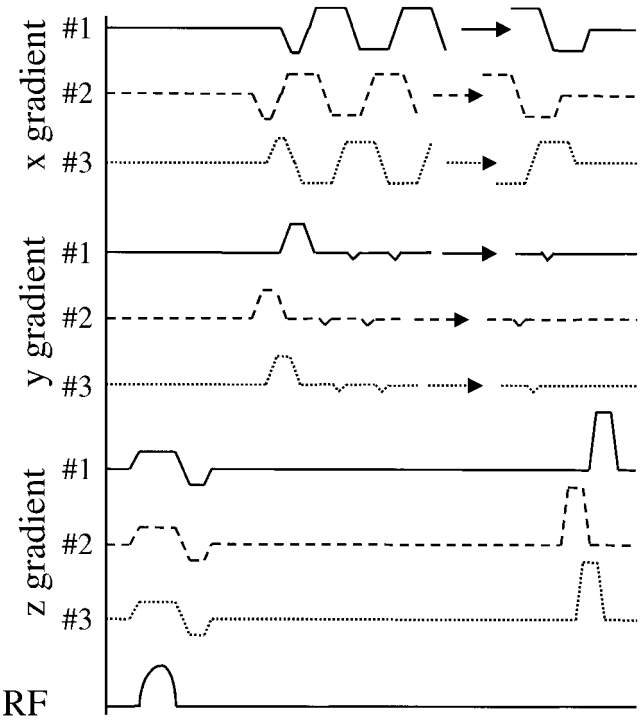

FIG. 1. Three-interleaf EPI pulse sequence diagram. For each interleaf, relative temporal delays and polarity changes of x (frequency encode), y (phase encode), and z (slice-select) gradient waveforms are shown for each of the three interleaves (labeled #1, #2, and #3). Interleaf #1 acquires the 1st k-space line and every third thereafter. Interleaves #2 and #3 acquire the 2nd and 3rd k-space lines and every third line thereafter, but the first acquired k-space line from each interleaf is discarded. To create a smooth T2* decay in the combined data set, interleaves #2 and #3 are temporally shifted such that their 2nd acquired k-space line is offset by 1/3 and 2/3 of the total time for one trapezoid of the readout gradient. Phase encoding occurs at the transitions between forward and reverse echos and is also temporally shifted in each interleaf. The slice-select gradient has a constant spoiler gradient after data acquisition to reduce residual transverse magnetization. Z-gradient and RF pulses for slice selection are identical for all interleaves.

due to gradient-dependent main field offsets, echo delays, and echo drifts. If the data alternate between forward and reverse echos in successive k-space lines, then $g_{lr}(n) = 1$ for n even, and $g_{lr}(n) = -1$ for n odd. This alternating pattern of echos produces a single ghost shifted ½ the FOV, which can be suppressed using image phase correction (12).

Multiple ghost artifacts, some shifted only a small distance from the parent image, occur with more complicated patterns of forward and reverse echos as a function of k_y. To derive the relation between the echo pattern, and the locations and complex amplitude factors of resulting ghosts, define

$$g_l(n) = \tfrac{1}{2}(1 + g_{lr}(n)) \quad \text{and} \quad g_r(n) = \tfrac{1}{2}(1 - g_{lr}(n)) \quad [2]$$

as functions identifying, respectively, the forward and reverse echos as a function of k-space line indexed by n. Set the spatial scale such that the object being reconstructed, $M(x,y)$, is defined at $N \times N$ integer-valued points (x, y) in the spatial domain. Following from Eq. [3] in ref. 12, the signal at points labeled by integers in k-space can then be written as

$$S(m, n) = (1/N^2) \sum_{x=-N/2}^{N/2-1} \sum_{y=-N/2}^{N/2-1} M(x, y) \times (g_l(n) \exp(i\theta(x, y)) + g_r(n) \exp(-i\theta(x, y))) \cdot \exp\left(-i \frac{2\pi}{N} mx\right) \exp\left(-i \frac{2\pi}{N} ny\right) \quad [3]$$

Regrouping terms, and carrying out an Inverse Fourier transform on Eq. [3], the reconstructed image, $M(x, y)$, can

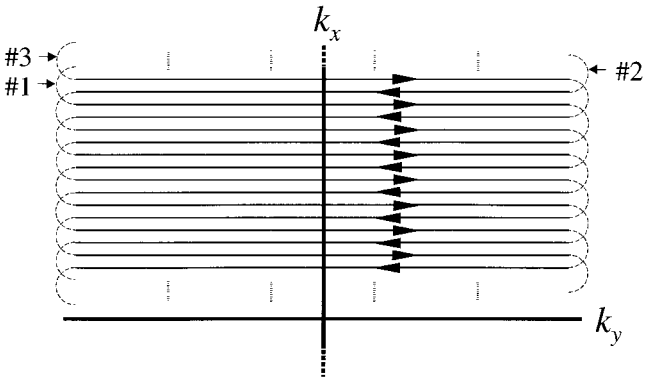

FIG. 2. Odd-number interleaf EPI. Three separate interleaves (labeled #1, #2, and #3) are combined to produce a *l-r-l-r-l-r-l-r-etc.* pattern of echos. In our implementation of 128 × 128 interleaved EPI, each interleaf acquires 44 k-space lines, yielding an excess of 4 lines that are discarded. Interleaf #1 acquires the 1st, 4th, 7th, etc. k-space lines (counting from 1 at top), interleaf #2 acquires the 2nd, 5th, 8th, etc. lines, and interleaf #3 acquires the 3rd, 6th, 9th, etc. lines. Interleaves #1 and #2 are initiated with a forward echo, while interleaf #3 is initiated with a reverse echo. The first acquired k-space line from interleaf #2, and the first acquired line from interleaf #3, are not used in the combined data set. Also, the last k-space line (131th in combined data set) from interleaf #3, and the last line from interleaf #1 (132th in combined data set) are discarded. Discarding the first k-space lines is based on the presumption that equilibrium phase errors may occur only after the first line, meaning that the 2nd and 3rd lines of the combined data set should not be acquired as the 1st line of one of the interleaves.

Table 1
Interleaved EPI Used for Figs. 4–7

No. of interleaves	Data matrix of each interleaf[1]	Resulting image matrix[1]
1	64 × 64	64 × 64
2	128 × 64	128 × 128
3	128 × 44	128 × 128
9	256 × 30	256 × 256

[1]Matrices are given as frequency encode × phase encode.

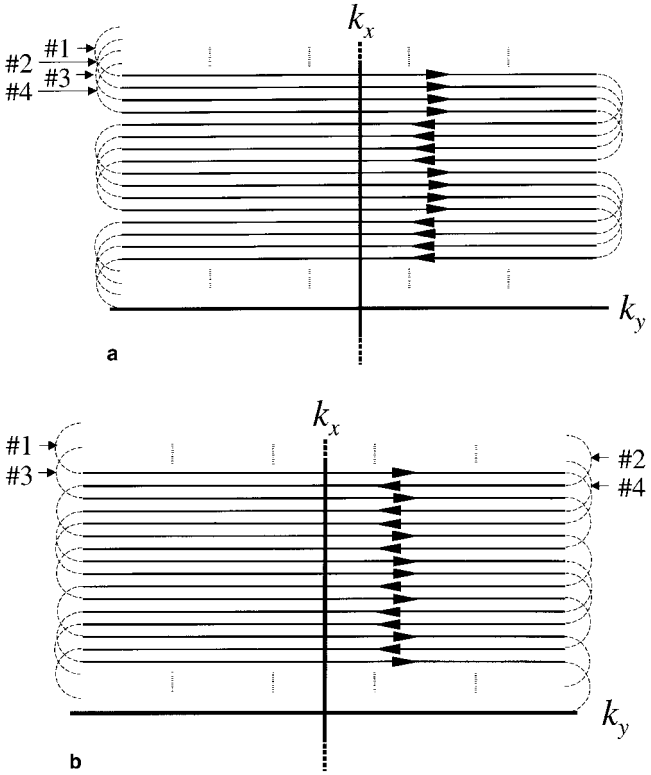

FIG. 3. Even-number interleaf EPI. In our implementation of 128 × 128 interleaved EPI, each interleaf acquires 32 k-space lines, and no lines are discarded. Four separate interleaves (labeled #1, #2, #3, and #4) are combined to produce different echo patterns. Each figure shows exactly two cycles of the smallest repeating pattern of the combined data set. **a:** A *l-l-l-l-r-r-r-r-etc.* pattern is formed by using interleaf #j (j = 1, 2, 3, or 4) to acquire the j^{th}, $(j + 4)^{th}$, $(j + 8)^{th}$, $(j + 12)^{th}$, etc. k-space lines. Each interleaf is initiated with a forward echo. **b:** A *l-r-l-r-r-l-r-l-etc.* pattern is formed by acquiring the same lines with each interleaf as in a, but initiating interleaves #2 and #4 each with a reverse echo. Locations and relative intensities of ghost artifacts from these patterns are computed using Eq. [8] with $h = 4$, and are listed in Table 2.

be written

$$\hat{M}(x, y) = M(x, y) \cos(\theta(x, y)) + \sum_{y'=-N/2}^{N/2-1} M(x, y') G_{lr}(y - y') \sin(\theta(x, y')) \quad [4]$$

where, similar to that in ref. 13, $G_{lr}(y - y')$ is defined as the Ghost Kernel given by

$$G_{lr}(y - y') \equiv (i/N) \sum_{n=-N/2}^{N/2-1} g_{lr}(n) \exp\left(-i \frac{2\pi}{N} n (y - y')\right) \quad [5]$$

Based solely on the periodicity of g_{lr} with n, the Ghost Kernel can also be written

$$G_{lr}(y - y') \equiv \sum_{j=-h}^{h-1} g_j \, \delta(y - y' - \Delta_j) \quad [6]$$

where $\Delta_j = N/2h\, j$, $j = -h+1, \ldots, h-1$, and δ a delta-like function defined by

$$\delta(y) \equiv (1/N) \sum_{n=-N/1}^{N/2-1} \exp\left(-i \frac{2\pi}{N} ny\right) = \begin{cases} 1 & \text{if } y = 0 \text{ Modulo } N \\ 0 & y \text{ integer} \neq 0 \end{cases} \quad [7]$$

Eq. [6] explicitly identifies each ghost location Δ_j and complex amplitude factor g_j. Substitution of Eq. [7] into Eq. [6], and comparison with Eq. [5], reveals the Fourier Transform relationship between $g_{lr}(n)$ and g_j:

$$g_{lr}(n) = -i \sum_{j=-h}^{h-1} g_j \exp\left(i \frac{2\pi}{N} n\Delta_j\right)$$
$$g_j = (i/2h) \sum_{n=-h}^{h-1} g_{lr}(n) \exp\left(-i \frac{2\pi}{N} n\Delta_j\right) \quad [8]$$

These equations show that the maximum number of ghosts is equal to $2h$, and the separation between the parent image and the two nearest (most-overlapping) ghosts are $\Delta_1 = N/2h$ and $\Delta_{-1} = -N/2h$ or $\pm 1/2h$ the FOV.

MATERIALS AND METHODS

Interleaved gradient-recalled EPI was implemented on a Signa Advantage 1.5 T MR System (GE Medical Systems,

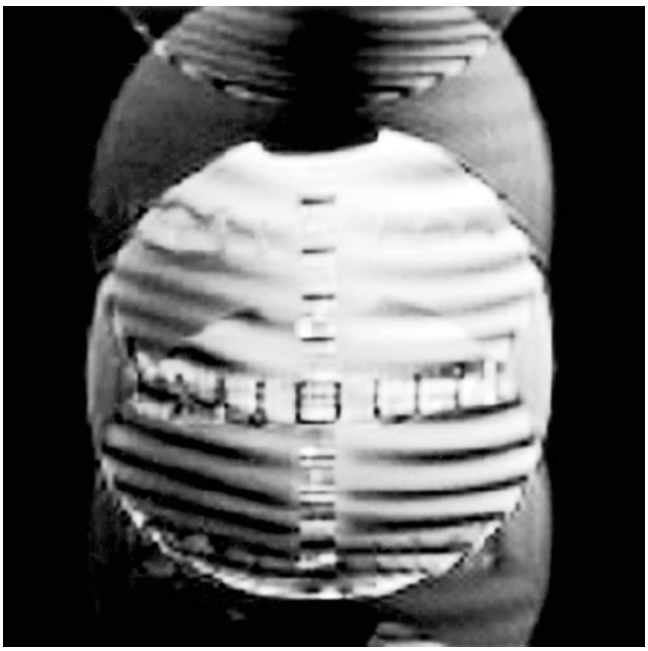

FIG. 4. Image of phantom using even-number interleaf EPI. In this implementation of 128 × 128 interleaved EPI, each of two interleaves acquired 64 k-space lines, and no lines were discarded. A *l-l-r-r-l-l-r-r-etc.* pattern of echos was formed by using interleaf #j (j = 1 or 2) to acquire the j^{th}, $(j + 2)^{th}$, $(j + 4)^{th}$, etc. k-space lines. Each interleaf was initiated with a forward echo. Locations and relative intensities of ghost artifacts in the image can be computed using Eq. [8] with $h = 2$. The locations Δ_j and complex amplitude factors g_j for these ghosts, denoted (Δ_j/N, g_j), (with N = 128 image matrix size) are (−½, 0), (−¼, ½i − ½), (¼, ½i + ½). These parameters are used in Eq. [4] to describe the image.

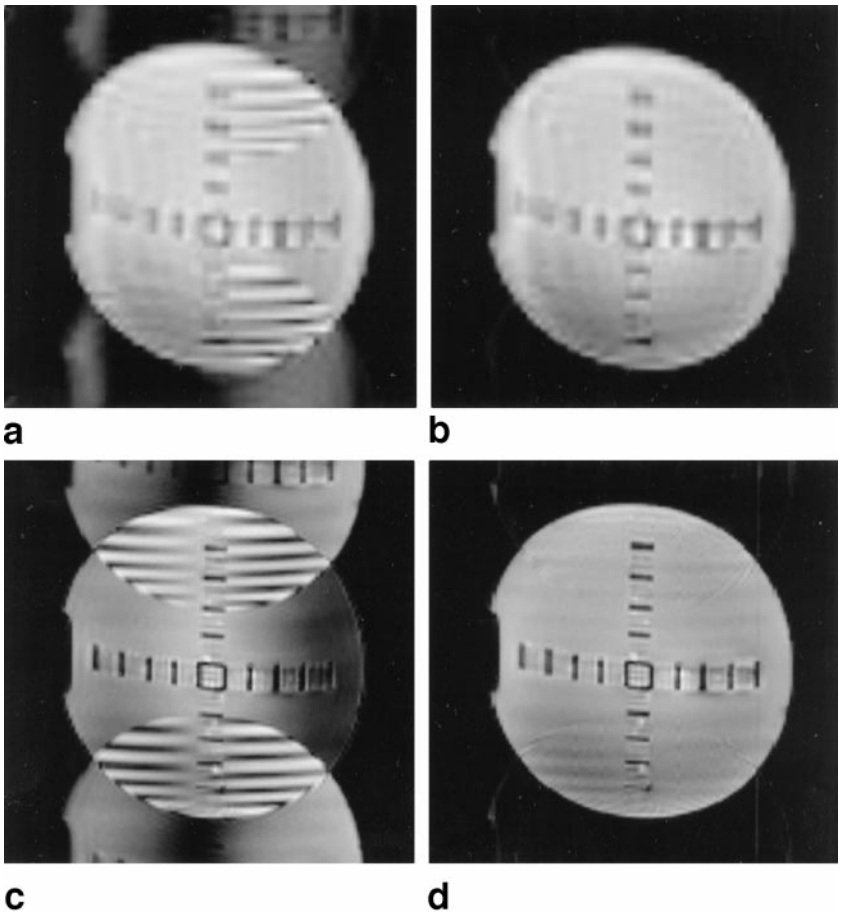

FIG. 5. Axial images of phantom obtained from single-shot and odd-number interleaf EPI, with and without ghost artifact reduction using image phase correction. **a:** 64 × 64 single-shot EPI with *l-r-l-r-l-r-l-r-etc.* pattern of echos. **b:** Image phase correction reduces average ghost intensity to 2.3% of average parent image intensity. **c:** 128 × 128 three-interleaf EPI, implementation described in text to generate *l-r-l-r-l-r-l-r-etc.* pattern of echos. **d:** Image phase correction reduces average ghost intensity to 4.3% of average parent image intensity.

Waukasha, WI) with Version 5.4 Genesis software platform. An insertable three-axis gradient and radiofrequency (RF) coil set (Medical Advances, Milwaukee, WI) was used, providing 2.0 g/cm peak gradient strength and 56 μsec rise time, and permitting 64×64 single-shot acquisitions in under 40 msec per image, and with duty cycle permitting up to 9 images/sec. Figure 1 shows the pulse sequence diagram for three interleaf EPI.

Specific interleaved EPI scans were performed on phantoms and normal subjects. Informed consent was obtained from all subjects. The following parameters were common to all scans: TE 40 msec, flip angle 90°, FOV 220 mm, slice thickness 6 mm, slice gap 2 mm, and number of locations 16. Phantom studies were run with TR 3.2 sec and subject studies with TR 2 sec. Table 1 shows the different interleaved scans that were performed and the resulting image matrix sizes. All images were linearly interpolated to 256 × 256 for display. After image phase correction, residual ghost intensity was measured as the average intensity of the image in the entire ghost-only region of the image, divided by the average intensity in the entire parent-only region of the image, and reported as a percentage.

RESULTS

Predictions of Theory

Typical interleaved EPI data sets assembled with forward and reverse echos grouped together produce ghosts that significantly overlap the parent image. Because image phase correction requires at least a one-pixel wide strip within the parent image that does not contain ghost, the technique cannot be applied with any such interleaved data sets (unless the FOVs were made impracticably large to separate the adjacent ghosts). However, if the interleaved EPI data could be arranged to have purely alternating forward and reverse echos (i.e., *l-r-l-r-l-r-l-r-etc.* pattern), then the resulting uncorrected reconstruction would have only one ghost shifted by ½ the FOV, and image phase correction could be applied.

Odd-Number Interleaf EPI

Even-number interleaf EPI cannot produce the required alternating pattern, but odd-number interleaf EPI can. The three interleaf EPI echo pattern is shown in Fig. 2. For comparison, two different even-number interleaf EPI echo patterns are shown in Fig. 3. Figure 3a shows a *l-l-l-l-r-r-r-r-etc*. pattern resulting from identical traversals of k-space of four interleaves. Figure 3b shows a *l-r-l-r-r-l-r-l-etc.* pattern resulting from alternating the direction of the traversal of interleaves #2 and #4. More detailed consideration reveals that the simple *l-r-l-r-l-r-l-r-etc.* pattern cannot be obtained from an even number of interleaves.

Experimental Verification

Figure 4 shows a 128 × 128 image obtained using two interleaf EPI (composed of two 128 × 64 interleaves). There are two ghosts shifted by ±¼ of the FOV, arising from the *l-l-r-r-l-l-r-r- etc.* pattern of phase errors. The ghost

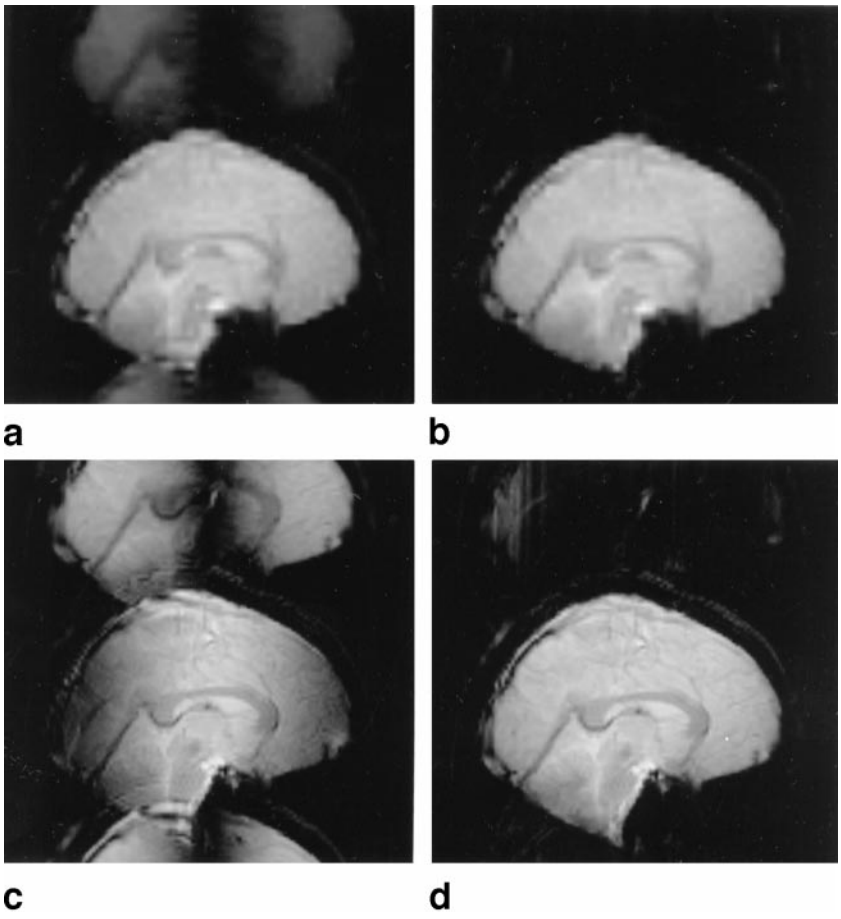

FIG. 6. Sagittal images of head obtained from single-shot and odd-number interleaf EPI, with and without ghost artifact reduction using image phase correction. **a:** 64 × 64 single-shot EPI with *l-r-l-r-l-r-l-r-etc.* pattern of echos. **b:** Image phase correction reduces average ghost intensity to 1.6% of average parent image intensity. **c:** 128 × 128 three-interleaf EPI, implementation described in text to generate *l-r-l-r-l-r-l-r-etc.* pattern of echos. **d:** Image phase correction reduces average ghost intensity to 5.6% of average parent image intensity.

shifted by ½ the FOV has zero amplitude. Ghost artifact reduction by image phase correction is not possible, because the parent image is almost everywhere overlapping with ghost. Figure 5a shows an image from 64 × 64 single-shot EPI, and Fig. 5b shows removal of the N/2 ghost using image phase correction. Figure 5c shows an image from 128 × 128 odd-number interleaf EPI composed of three 128 × 44 interleaves and confirms that the sequence causes only a single ghost shifted by ½ the FOV. Figure 5d confirms that image phase correction largely suppresses this ghost. Figure 6 displays similar results obtained in the sagittal plane on a normal subject. Figure 6a shows an image from 64 × 64 single-shot EPI with a single ghost artifact, and Fig. 6b shows removal of the ghost using image phase correction. Figure 6c shows an image from 128 × 128 odd-number interleaf EPI composed of three 128 × 44 interleaves, and confirms that the sequence causes only a single ghost shifted by ½ the FOV. Figure 6d confirms that image phase correction largely suppresses this ghost. Figure 7 shows images from 256 × 256 odd-number interleaf EPI (composed of nine 256 × 30 interleaves). These images confirm that large odd-number interleaf EPI produces only a single ghost shifted by ½ the FOV.

Comparison of Even- and Odd-Number Interleaf EPI

Table 3 lists possible desired image resolutions and compares data acquisition time, number of slices, and temporal

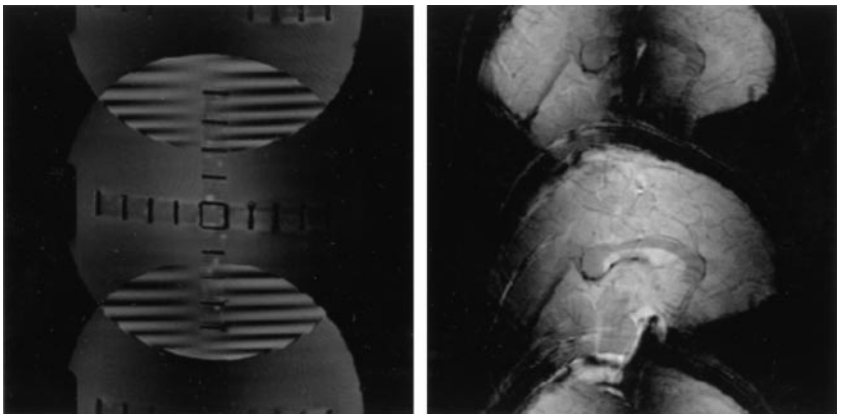

FIG. 7. Axial phantom (left) and sagittal head (right) images obtained from odd-number interleaf EPI. 256 × 256 combined data set with *l-r-l-r-l-r-l-r-etc.* pattern of echos was acquired using nine 256 × 30 interleaves. Interleaf #j, j = 1,2, ..., 9, was used to acquire the j^{th}, $(j + 9)^{th}$, $(j + 18)^{th}$, $(j + 27)^{th}$ k-space line (number from 1 starting at top), and interleaves #3, #5, #7, and #9 were initiated with reverse echos (all others were initiated with forward echos). The first acquired k-space lines were discarded in interleaves #2 through #9, as were the last acquired lines in interleaves #1, #5 through #9. The lack of ghosts, other than that shifted by ½ the FOV, validates the assumption that phase errors represented by $\pm\theta(x)$ are the same in separately acquired interleaves.

Table 2
Ghost Complex Amplitude Factors in $h = 4$ Interleaved EPI Shown in Fig. 3*

Ghost location offset	*l-l-l-l-r-r-r-r-*etc. pattern	*l-r-l-r-r-l-r-l-*etc. pattern
$-1/2$	0	0
$-3/8$	$0.25\,i - 0.10$	$0.25\,i + 0.60$
$-1/4$	0	0
$-1/8$	$0.25\,i - 0.60$	$0.25\,i + 0.10$
0	0	0
$1/8$	$0.25\,i + 0.60$	$0.25\,i - 0.10$
$1/4$	0	0
$3/8$	$0.25\,i + 0.10$	$0.25\,i - 0.60$

*Ghost position offsets are Δ_j, $j = -h, -h+1, \ldots, h-1$, as defined in Eq. [6], and are listed here as fractions of the FOV and relative to the location of parent image. Ghost complex amplitude factors are g_j, as defined in Eqs. [6] and [8]. The echo pattern repeats across the phase encode direction, and the amplitude factors are calculated assuming that the first letter of the pattern gives the direction at $k_y = 0$. Note that both patterns generate ghosts close to the parent image at $\pm 1/2h = \pm 1/8$ the FOV.

resolution that can be obtained using odd number versus even-number interleaf EPI. The table entries are computed with fMRI neural activation experiments in mind, in which temporal resolution of not worse than 3000 msec would typically be required. For a given spatial resolution and number of interleaves, the right two columns give the number of distinct slice locations that can be obtained (constrained by 3000 msec temporal resolution), and the required TR (defined as the time interval between acquisition of sequential interleaves at a given slice). The table reveals that odd-number interleaf EPI is complementary to even-number interleaf EPI, and one may argue that either set alone would be sufficient for the vast majority of fMRI experiments.

DISCUSSION

Based on our experience, reference scans are not as reliable as image phase correction (12). Not infrequently, poor reference scans make the image quality worse by virtue of poor estimation of the phase errors in the image data. Reference scans will be proportionally more unreliable in interleaved EPI when separate phase corrections are required for each interleaf. A recent comparison (14) between image reference correction with two established reference scan methods (5,11) showed that image phase correction reduced artifact more.

If the user is willing to increase the acquisition time, then the problem of overlapping ghost artifact can be avoided by either 1) doubling the FOV while maintaining

Table 3
Comparison of Even- and Odd-Number Interleaf EPI

Data matrix (freq × ph)	No. of leafs	k-lines/ leaf	Time/leaf (ms)	k-lines acquired	k-lines discarded	No. of slices with 3000 ms temporal resolution	Required TR (ms) for 3000 ms temporal resolution
64 × 64	1	64	39.9	64	0	27	3000
128 × 128	2	64	72.7	128	0	7	1500
128 × 128	3	44	50.0	132	4	7	1000
128 × 128	4	43	36.4	128	0	7	750
128 × 128	5	27	30.7	135	7	7	600
192 × 128	3	44	72.5	132	4	4	1000
192 × 128	4	32	52.7	128	0	5	750
192 × 128	5	27	44.5	135	7	4	600
192 × 128	6	23	37.9	138	10	4	500
192 × 192	4	48	79.1	192	0	3	750
192 × 192	5	40	65.9	200	8	3	600
192 × 192	6	32	52.7	192	0	3	500
192 × 192	7	29	47.8	203	11	3	428
256 × 192	6	32	69.1	192	0	2	500
256 × 192	7	29	62.6	203	11	2	428
256 × 192	8	24	51.8	192	0	2	375
256 × 192	9	23	49.7	207	15	2	333
256 × 128	4	32	69.1	128	0	3	750
256 × 128	5	27	58.3	135	7	3	600
256 × 128	6	23	49.7	138	10	3	500
256 × 128	7	20	43.2	140	12	3	428
256 × 256	8	32	69.1	256	0	1	375
256 × 256	9	30	64.8	270	14	1	333
256 × 256	10	27	58.3	270	14	1	300
256 × 256	11	25	54.0	275	19	1	272

Table lists only those acquisitions producing 30 ms < time/leaf < 80 ms. Headings: Time/leaf: computed using 8 us sampling rate and 56 us gradient rise time. Data matrix: combined raw data array size, freq: frequency encode direction, ph: phase encode direction; k-lines discarded: Excess k-space lines not needed for reconstruction; No. of slices . . . : Estimated from time/leaf and duty cycle limit: of local gradient coil (LGC); Required TR (ms) . . . : TR needed to acquire combined data set.

the pixel size by doubling the number of phase encode steps; 2) retaining the FOV and acquiring lines only in one direction with an asymmetric gradient waveform as in ABEST (15,16); or 3) doubling the number of phase encode steps using a standard readout waveform and performing two reconstructions, first using only the forward lines and then only the reverse lines, with image averaging to improve the signal-to-noise ratio (e.g., ref. 17). The odd-number interleaf EPI is valuable because in most EPI applications it is an optimal strategy to match the FOV to the object size and minimize the number of phase encode steps, to make image acquisition as rapid and with as few interleaves as possible, while avoiding image wraparound. This strategy reduces artifacts from physiological motion and maximizes temporal resolution for imaging dynamical processes.

REFERENCES

1. McKinnon GC. Ultrafast interleaved gradient echo planar imaging on a standard scanner. Magn Reson Med 1993;30:609–616.
2. Butts K, Riederer SJ, Ehman RL, Thompson RM, Jack CR. Interleaved echo planar imaging on a standard MRI system. Magn Reson Med 1994;31:67–72.
3. Feinberg DA, Oshio K. Phase errors in multi-shot echo planar imaging. Magn Reson Med 1994;32:535–539.
4. Slavin GS, Butts K, Rydberg JN, Jack CR, Riederer SJ. Dual-echo interleaved echo-planar imaging of the brain. Magn Reson Med 1995;33: 264–270.
5. Bruder H, Fischer H, Reinfelder HE, Schmitt F. Image reconstruction for echo planar imaging with nonequidistant k-space sampling. Magn Reson Med 1992;23:311–323.
6. Wong EC. Shim insensitive phase correction for EPI using a two echo reference scan. In: Proceedings of the SMRM, 11th Annual Meeting, Berlin, Germany, 1992. p 4514.
7. Jesmanowicz A, Wong EC, Hyde JS. Phase correction for EPI using internal reference lines. In: Proceedings of the SMRM, 12th Annual Meeting, New York, 1993. p 1239.
8. Maier JK, Vevrek M, Glover GH. Correction of NMR data acquired by an echo planar technique. US Patent #5,151,656 (1992).
9. Jesmanowicz A, Wong EC, Hyde JS. Self-correcting EPI reconstruction algorithm. In Proceedings of the SMR, 3rd Annual Meeting, Nice, France, 1995. p 619.
10. Mandeville JB, Weisskoff RM, Garrido L. Reduction of eddy-current induced Nyquist ghosts and sampling artifact. In: Proceedings of the SMR, 3rd Annual Meeting, Nice, France, 1995. p 613.
11. Hu X, Le TH. Artifact reduction in EPI with phase encoded reference scan. Magn Reson Med 1996;36:166–176.
12. Buonocore MH, Gao L. Ghost artifact reduction for echo-planar imaging using image phase correction. Magn Reson Med 1997;38:89–100.
13. Reeder SB, Atalar E, Bolster BD, McVeigh ER. Quantification and reduction of ghosting artifacts in interleaved echo-planar imaging. Magn Reson Med 1997;38:429–439.
14. Clare S, Bowtell R, Morris P. Ghost artefact in fMRI: comparison of techniques for reducing the N/2 ghost. In: Proceedings of the ISMRM, on CD-ROM. 1998. p 2137.
15. Feinberg DA, Turner R, Jakab PE, von Kienlin M. Echo-planar imaging with asymmetric gradient modulation and inner-volume excitation. Magn Reson Med 1990;13:162–169.
16. Hennel F, Nedelec J-F. Interleaved asymmetric echo-planar imaging. Magn Reson Med 1995;34:520–524.
17. Posse S, Tedeschi G, Risinger R, Ogg R, Le Bihan D. High speed ^{1}H spectroscopic imaging in human brain by echo planar spatial-spectral encoding. Magn Reson Med 1995;33:34–40.